Preparation and Characterization of UV-Curable MPS-modified Silica Nanocomposite Coats

Fusheng Li,[1] Shuxue Zhou,[1] Limin Wu[1,2]

[1]*Department of Materials Science, The Advanced Coatings Research Center of China Educational Ministry, Fudan University, Shanghai 200433, People's Republic of China*
[2]*College of Chemistry and Materials Science, Hubei University, Wuhan 430062, People's Republic of China*

Received 27 March 2005; accepted 1 May 2005
DOI 10.1002/app.22143
Published online in Wiley InterScience (www.interscience.wiley.com).

ABSTRACT: A series of UV-curable nanocomposites were prepared with 3-(trimethoxysilyl) propyl methacrylate (MPS) modified nanosilica under the initiation of 2,2-dimethoxy-1,2-diphenylethan-1-one. It was found that MPS-modified nanosilica together with free MPS could form transparent nanocomposite coats. As the particle size of nanosilica increased, the photopolymerization rate, final double bond conversion, and tack-free time of nanocomposites increased while the surface roughness, glass-transition temperature, and UV absorbance of nanocomposites decreased. © 2005 Wiley Periodicals, Inc. J Appl Polym Sci 98: 2274–2281, 2005

Key words: nanosilica; nanocomposite coats; UV-curable; photopolymerization; crosslinking

INTRODUCTION

It is well known that nanocomposites can combine advantages of organic polymers (flexibility, ductility, dielectric strength, etc.) and the inorganic materials (rigidity, high thermal stability, UV shielding property, high refractive index, etc.). Moreover, they usually contain some special properties of nanoparticles, and consequently, can be widely used in many fields, such as plastics, rubbers, coatings, inks, etc.[1–5] UV-curable process has some advantages (fast, environment friendly, energy saving, etc.), and can be used to cure nanocomposites for coatings, printings, inks, adhesives, and for other fields.[6–10]

There were many reports on UV-curable nanocomposites,[11–18] but most of them were focused on the synthesis and characterization of nanocomposites containing clay as nanofillers.[11–14] Only very limited papers dealt with composites containing nanosilica particles. Among them, Bauer and coworkers[6,16,17] successfully prepared UV-curable nanocomposite coats with high scratch and abrasion resistance, using trimethoxysilyl-terminated propyl methacrylate-modified nanosilica as the fillers. Muh et al.[7] first synthesized UV-curable hybrid nanocomposite through a sol–gel process of alkoxysilane-containing bismethacrylate-based monomers. Xu et al.[19] introduced nanosilica fillers into biphenyl A epoxy acrylate directly and successfully prepared corresponding nanocomposites with improved thermal stability and mechanical properties. However, all these UV-curable nanocomposites contained reactive dilutes (e.g., TMPTA, HDDA) or oligomers (e.g., epoxy acrylate, urethane acrylate) or both of them in UV-curable formulation. The nanocomposite films or coats could be formed via the crosslinking reaction of oligomers and/or reactive dilutes, and nanosilica particles only acted as fillers.

The aim of this study is to try to explore the possibility of a novel UV-curable nanocomposite film, in which nanosilica particles were firstly modified by 3-(trimethoxysilyl) propyl methacrylate (MPS) and then condensed. The MPS-modified nanosilica, functionalized as the sole crosslinking agent, and residual free MPS were then cured to form coats by UV ray under the photoinitiator; no other reactive dilutes or oligomers were used in the whole process. The photopolymerization kinetics, tack-free time, morphology, thermal stability, and optical property of the nanocomposites with various size nanosilica were investigated by Fourier transform infrared spectrophotometer (FTIR), scanning electron microscope (SEM), atomic force microscope (AFM), differential scanning calorimetry (DSC), and UV–vis spectrophotometer, respectively.

EXPERIMENTAL

Materials

Tetraethyl orthosilicate (TEOS) and MPS were purchased from Shanghai Huarun Chemical Company of

Correspondence to: L. Wu (lxw@fudan.ac.cn).
Contract grant sponsor: National "863" Program, Shanghai Special Nano Foundation, the Doctoral Foundation of University, Trans-century Outstanding Talented Person Foundation of China Educational Ministry, Key Project of China Educational Ministry.

TABLE I
Recipes for Preparation of Nanosilica with Different Particle Size

	Recipe (mol)			
Nanosilica (nm)	TEOS	NH_3	H_2O	EtOH
30	1	0.15	2.5	9
40	1	0.20	2.5	9
50	1	0.25	2.5	9
75	1	0.30	2.5	9

China. Absolute ethanol (EtOH) and ammonia solution (25–28% ammonia content) were purchased from Shanghai Chemical Reagent Corp. 2, 2-dimethoxy-1,2-diphenylethan-1-one (Irgacure 651) is a gift of Ciba Specialty Chemicals. All these materials were used without further purification.

Preparation and modification of nanosilica

Colloidal silica microspheres with mean size from 30 to 75 nm were prepared according to the recipes, as shown in Table I. In brief, TEOS and partial EtOH were first charged into three-necked round bottom flask, and then the residual EtOH, deionized water, and ammonia were dropped within 0.5 h and continued to react at 50°C for 24 h under stirring. Then, MPS was added based on the 1 : 5*M* ratio of MPS/TEOS, and the reaction was continued for another 6 h. The resulted nanosilica sol was condensed under vacuum at 50°C to remove almost all the water and ethanol. Finally, a liquid mixture of MPS-modified nanosilica particles and residual MPS was obtained for further use.

Preparation of nanocomposite coats

The mixture of MPS-modified nanosilica particles and residual free MPS was added by 2 wt % photoinitiator based on the solid mass of mixture, then cast on glass substrates, and cured by an UV curing apparatus (UV Crosslinker, Spectroline Company) with intensity of 2.2 mW/cm^2 and various exposure time in the air. The thickness of obtained nanocomposite coat was in the range of 20–40 μm. The nanosilica content in all nanocomposites was 65 $\pm$ 1 wt % based on the TGA measurement.

Characterization of nanosilica and nanocomposites

Particle size analysis

The particle size of nanosilica dispersed in ethanol was determined by N4 Plus submicron particle size analyzer (Beckman Coulter Company, Fullerton, CA). The SDP (size distribution processor) model was used to analyze the data.

FTIR analysis

The C═C bond peak at 1636 cm^{-1} in FTIR spectrum was adopted to monitor photopolymerization kinetics, using MAGNA-IR® 550 spectrometer (Nicolet Instruments, Madison, WI). The MPS-modified nanosilica powders after centrifuging and drying, and the condensed sols deposited between two NaCl crystal windows in thin layer exposed to UV ray (intensity ~2.2 mW/cm^2) for various time intervals were analyzed by FTIR spectrometer.

TGA analysis

TGA curves were obtained using a thermogravimetric apparatus (SDT 2960, TA Instrument, New Castle, DE) to investigate the inorganic fraction in modified nanosilica. The MPS-modified nanosilica powders after multicentrifuging and drying, and was used for TGA measurement. The temperature was ranged from room temperature to 900°C, with a heating rate of 10°C/min in the air flow.

SEM observation

The nanocomposite coats were prepared by freshly breaking in liquid nitrogen and coated using aurum spattering, and then observed by SEM (XL30, Philips Corp., The Netherlands).

AFM measurement

AFM images of the hybrid films were recorded by a Multimode Nanoscope III instrument (NSK Ltd., Japan) in tapping mode, with a silica probe (NSC 11) and a frequency of 2 Hz. The scan size varied between 2 and 5 μm and the roughness analysis was performed on 2 $\times$ 2 μm^2 and 5 $\times$ 5 μm^2 images. The root square roughness value (Rq) is the standard deviation of the *Z* values (the height) calculated within the given area as:

$$Rq = \sqrt{\frac{\Sigma(Z_i - Z_{ave})^2}{N}},$$

where Z_i is the current *Z* value, Z_{ave} is the average of the *Z* values, and *N* is the number of data points within the given area.[20]

DSC analysis

DSC thermograms were recorded using TA DSC at a heating rate of 10°C/min under a nitrogen atmosphere in the range of 0–120°C.

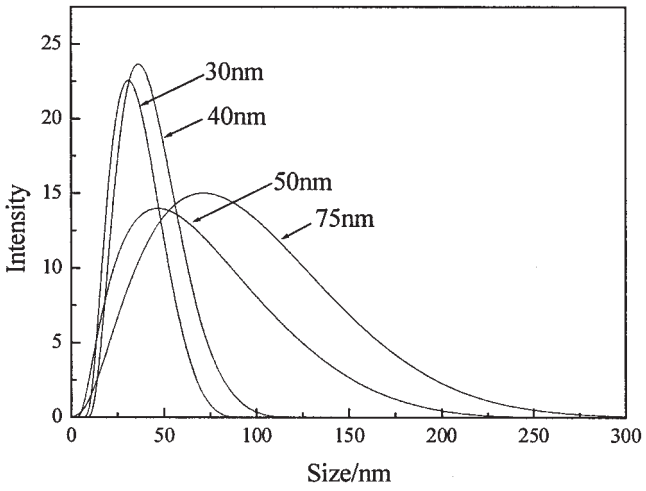

Figure 1 Particle size and its distribution in various colloidal nanosilica.

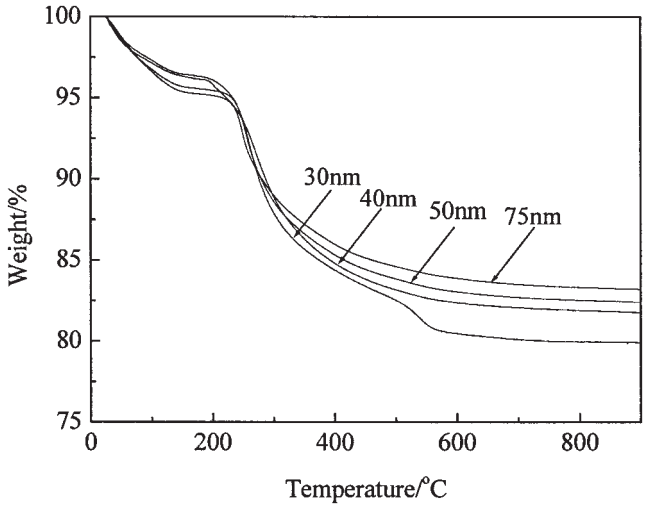

Figure 3 TGA curves for various MPS-modified nanosilica.

UV–vis spectra

The absorbance and transmittance spectra of the nanocomposite films in the range of 190–700 nm wavelength light were recorded by a UV–vis spectrophotometer (Hitachi UV-3000, Japan).

RESULTS AND DISCUSSION

Preparation of MPS-modified nanosilica particles

A series of nanosilica at mean particles size of 30, 40, 50, and 75 nm, as indicated in Figure 1, were prepared *via* sol–gel method on the basis of the recipes in Table I, and then modified by MPS. Excessive MPS was used here to get a maximum modification effect. The FTIR spectra of MPS-modified nanosilica powders were shown in Figure 2. Relative to the spectrum of unmodified nanosilica particles, a new absorbing peak at 1636 cm^{-1} assigned to C═C vibration was observed in the spectra of MPS-modified nanosilica particles, indicating MPS has been successfully attached to the surfaces of nanosilica particles. Figure 3 illustrated the TGA results of modified nanosilica in different particle size; the smaller the nanosilica was, the more the grafted MPS were. This was certainly related to the —OH group quantity on the unmodified nanosilica surface; the smaller the unmodified nanosilica was, the more the group of —OH were. Thus, the possibility of MPS grafted on the nanosilica surface increased, and correspondingly, the grafting yield increased. Then, it is possible to control the MPS grafting yield on the nanosilica surface, by varying particle size of unmodified nanosilica. The MPS-modified nanosilica was then condensed under vacuum at 50°C to remove all water and ethanol. Otherwise, thermal pretreatment process

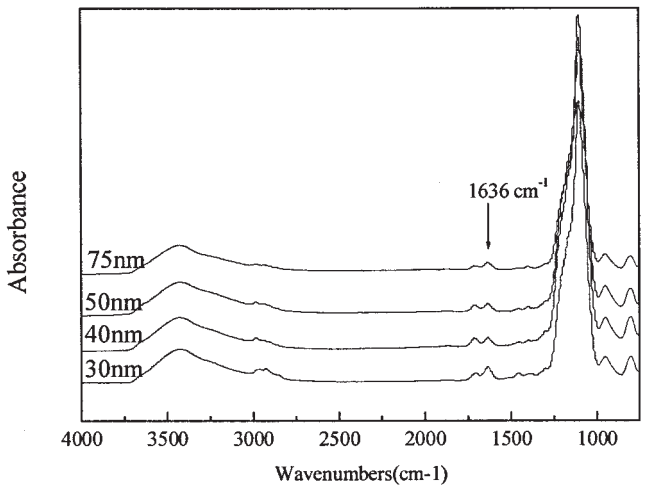

Figure 2 FTIR spectra of different MPS-modified nanosilica.

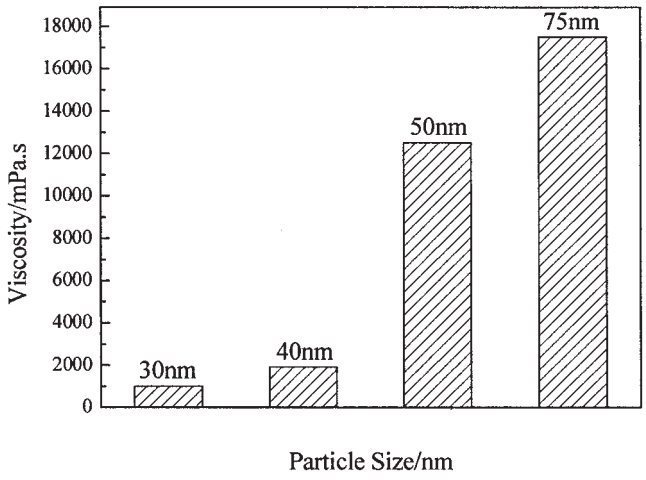

Figure 4 The viscosity of condensed nanosilica sols.

to evaporate them was needed before UV curing process.

After condensation, the nanosilica sols were transformed into viscous liquid. The viscosity of these condensed nanosilica sols was measured at 25°C and shown in Figure 4. It could be seen that the viscosity increased markedly with increasing nanosilica particle size. This is probably because larger nanosilica particles had much less MPS grafted just as indicated by TGA, decreasing the compatibility between nanosilica particles and MPS molecules.

Photopolymerization kinetics of nanocomposites

The mixture of MPS and MPS-modified nanosilica could be cured by two modes under UV irradiation, namely condensation of nanosilica induced by the heat produced during UV curing process or radical photopolymerization of MPS and MPS-modified nanosilica. Since the change in temperature was very little (within 2°C) during UV curing process, the condensed silica sol mixture should be fully cured by radical photopolymerization mechanism, just as depicted in Figure 5. Thus, the photopolymerization mechanism of condensed silica sol mixture could be studied using FTIR spectra.

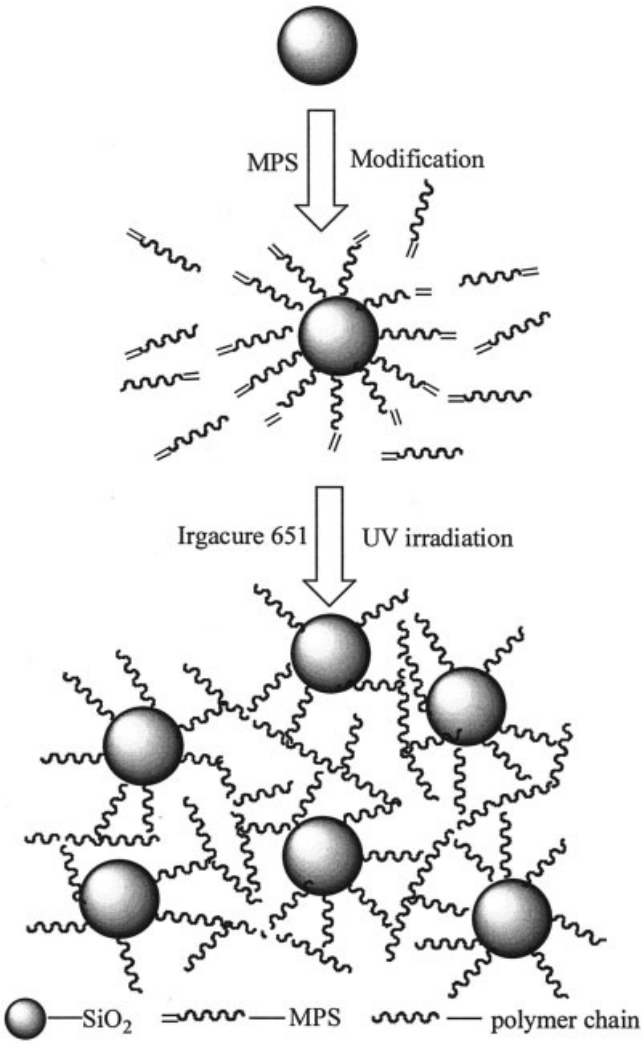

Figure 5 Schematic curing mechanism of condensed silica sol mixture under UV irradiation.

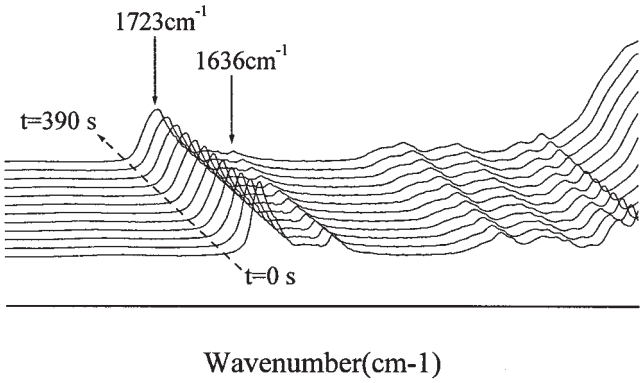

Figure 6 The typical FTIR spectra of nanocomposite coats cured under various UV irradiation time.

Figure 6 demonstrates the typical FTIR spectra of UV-curable nanocomposite coats, with different irradiation time. It was found that the intensity of the peak at 1636 cm^{-1} for C═C stretching absorbance decreased with increasing exposure time under UV irradiation. Since the peak at 1636 cm^{-1} was well separated from the other peaks, it was usually used to quantify the conversion of C═C bond in UV-curable process, and another peak at 1723 cm^{-1} due to C═O stretching absorbance was designated as the reference peak for its invariability.[21,22] Thus, the conversion of C═C bond could be calculated according to the following equation:

$$C\ (\%) = 100 \times (1 - A_t S_0 / A_0 S_t) \qquad (1)$$

where A_t and A_0 were the areas of the 1636 cm^{-1} peak and S_t and S_0 are the areas of the 1723 cm^{-1} peak at time t, and $t = 0$, respectively.

Figure 7 demonstrates the conversion curves of nanocomposite coats containing different nanosilica. It could be found that the nanocomposite coats have analogous photopolymerization kinetics to traditional UV-curable coats. The polymerization rate increased quickly at the beginning due to acceleration effect, and then slowed down due to the vitrification effect, which was not difficult to understand considering that MPS-modified nanosilica acted as multifunctional crosslinking component in these nanocomposites system. Figure 8 shows the polymerization rate against irradiation time. The larger the particle size was, the shorter the exposure time to the maximum rate was. The nanocomposite with 75-nm nanosilica reached the

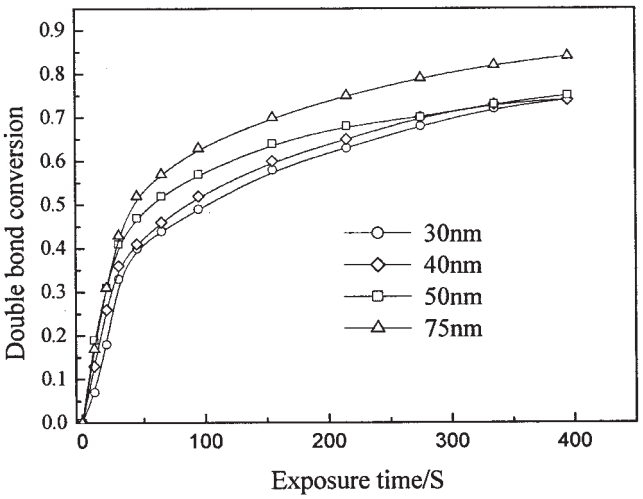

Figure 7 The double bond conversion with UV irradiation time for the coatings with different nanosilica (light intensity, 2.2 mW/cm^{-2}; film thickness: 20 μm).

maximum polymerization rate at only exposing around 12 s. This was probably because of the high initial viscosity of the nanocomposite containing large nanosilica, which was favorable for autoacceleration from the onset of the photopolymerization. Therefore, both photopolymerization rate and final double bond conversion of nanocomposite increased with increasing nanosilica particle size. This was probably because the smaller nanosilica particles had more MPS grafted, as indicated in Figure 3, which led to higher crosslinking degree at the beginning of UV irradiation comparing with the larger nanosilica particles. The high crosslinking network cumbered the mobility of monomers or oligomers, decreasing polymerization rate and final conversion.

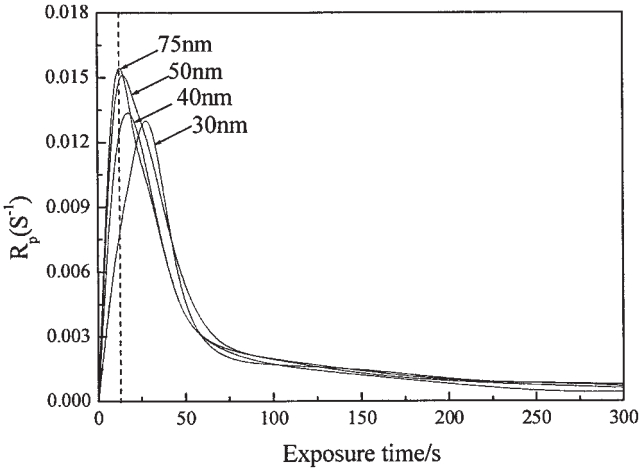

Figure 8 The photopolymerization rate with UV irradiation time for the coatings with different nanosilica (derived from Fig. 7).

TABLE II
Tack-Free Time for Different Nanocomposites

Coats with varied nanosilica (nm)	30	40	50	75
Tack-free time (s)	10	20	150	230

Tack-free time for nanocomposite coats

Tack-free time, a parameter to characterize the curing level on the surface of a film, was usually used to evaluate surface curing speed of coatings in the presence of oxygen.[23] Table II summarizes the tack-free time of coats with different size nanosilica. It was very strange that the tack-free time increased with increasing nanosilica particle size. Since the viscosity of the system, the photopolymerization rate, and final double bond conversion of nanocomposite coats increased with increasing nanosilica particle size, the tack-free time was supposed to decrease due to the lowering oxygen inhibition effect according to the traditional UV-curable coatings.[24] The possible reason could be explained as follows: although both photopolymerization rate and final conversion of nanocomposites increased with increasing nanosilica particle size, this did not that mean the crosslinking density of nanocomposite coats also aggrandized. In fact, the larger the nanosilica particles were, the less the MPS grafted on nanosilica were, and the more the free MPS molecules were. However, MPS had only one double bond per molecule, and thus could not contribute to formation of three-dimension network alone. Therefore, larger nanosilica particles meant lower crosslinking density, since MPS-modified nanosilica played a main role in the formation of three-dimensional network, which was distinctly different from the systems having functionalized nanosilica as filler. The decreasing crosslinking density indicated more oxygen inhibition effect as with increasing nanosilica particle size, extending the tack-free time.

Morphology of nanocomposites

The transparency of cured coats indicated no macroscopic phase separation occurred and no silica domains greater than the wavelength of visible light. The SEM pictures of cross sections of nanocomposites films, as shown in Figure 9, illustrated that nanosilica particles were evenly dispersed in organic matrix and no obvious aggregates and cracks were observed irrespective of particle size, suggesting that the preparing method of UV-curable nanocomposite coats proposed in this study was feasible for preparing nanocomposites with super-high nanosilica content. Moreover, the nanocomposites with small nanosilica seemed to form much more homogenous cross section than those with large nanosilica probably due to better compatibility between small nanosilica with matrix.

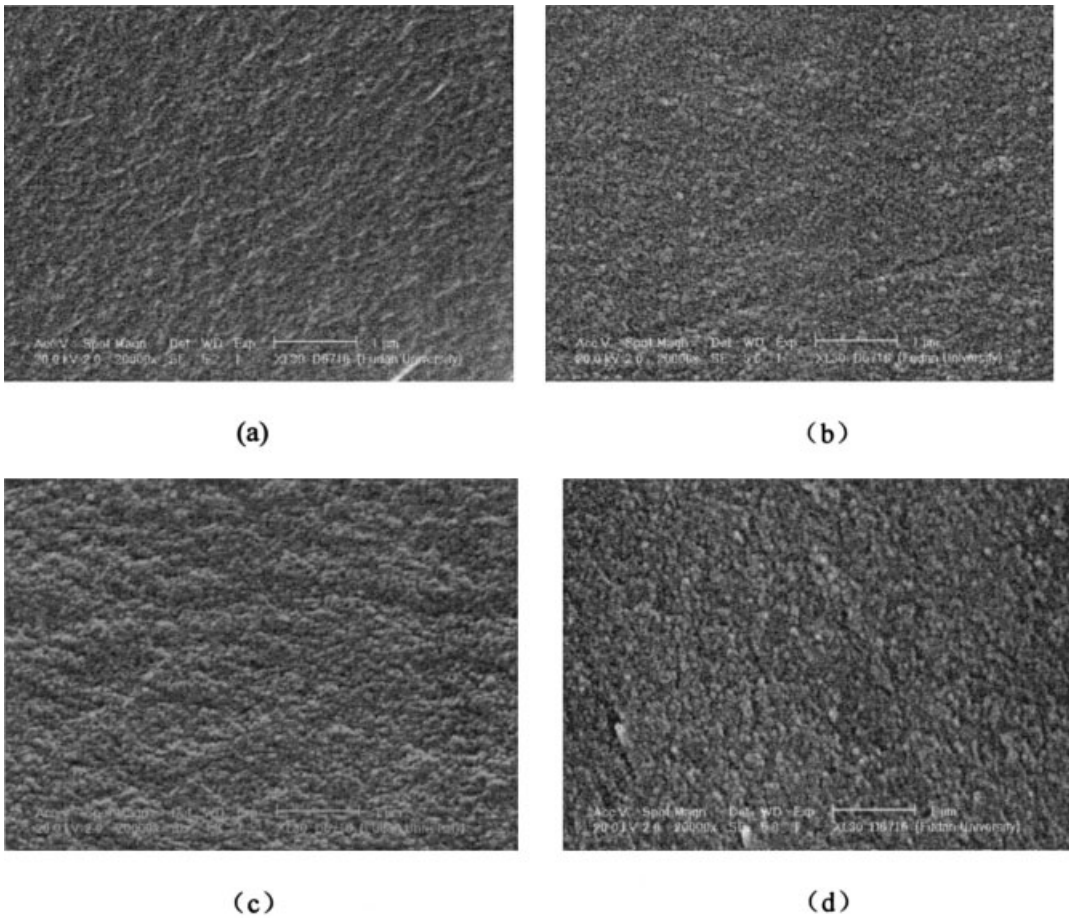

Figure 9 The SEM pictures of cross sections of nanocomposite films with various nanosilica.

Surface morphology of nanocomposites

The three-dimension AFM images of nanocomposite coats were shown in Figure 10 and the surface roughness was summarized in Table III. Both Figure 10 and Table III show that the surfaces of nanocomposite coats were relatively smooth at surface roughness below 3 nm, and unexpectedly, the roughness of nanocomposite coats gradually decreased with increasing nanosilica particle size. The systems with low viscosity and small size nanosilica theoretically should lead to smoother surface of nanocomposite coats because of good leveling ability in comparison with those with high viscosity and large size nanosilica. This was probably attributed to the fact that low viscosity availed the immigration of small nanosilica particles towards the surfaces of coats before UV irradiation, increasing the surface roughness of the nanocomposite coats.

Thermal analysis

Figure 11 presents DSC curves of nanocomposites. All nanocomposites had relatively high glass-transition temperature (T_g) because of their super-high nanosilica content. The T_g decreased, as the particle size of nanosilica increased because of reducing crosslinking density of nanocomposites, just as discussed by tack-free time.

Optical property of nanocomposite coats

Figure 12 illustrates the UV–vis spectra of nanocomposite coats. More than 90% of transmittance for all nanocomposites were observed in visible wavelength range (400–700 nm), indicating that introduction of nanosilica did not reduce the transmittance of UV-cured coats. However, the nanocomposites had obvious absorbance in UV range, especially below 300 nm, and the transmittance of nanocomposites in this range markedly decreased due to quantum size effect of nanosilica particles. Moreover, the smaller the nanosilica particles were, the greater the UV absorbance was and the lower the UV transmittance was. Therefore, the nanocomposite coats prepared in this study had excellent UV shielding property and transparency as well.[25]

CONCLUSIONS

This paper presented a preparation method for UV-curable nanocomposite coats, in which nanosilica parti-

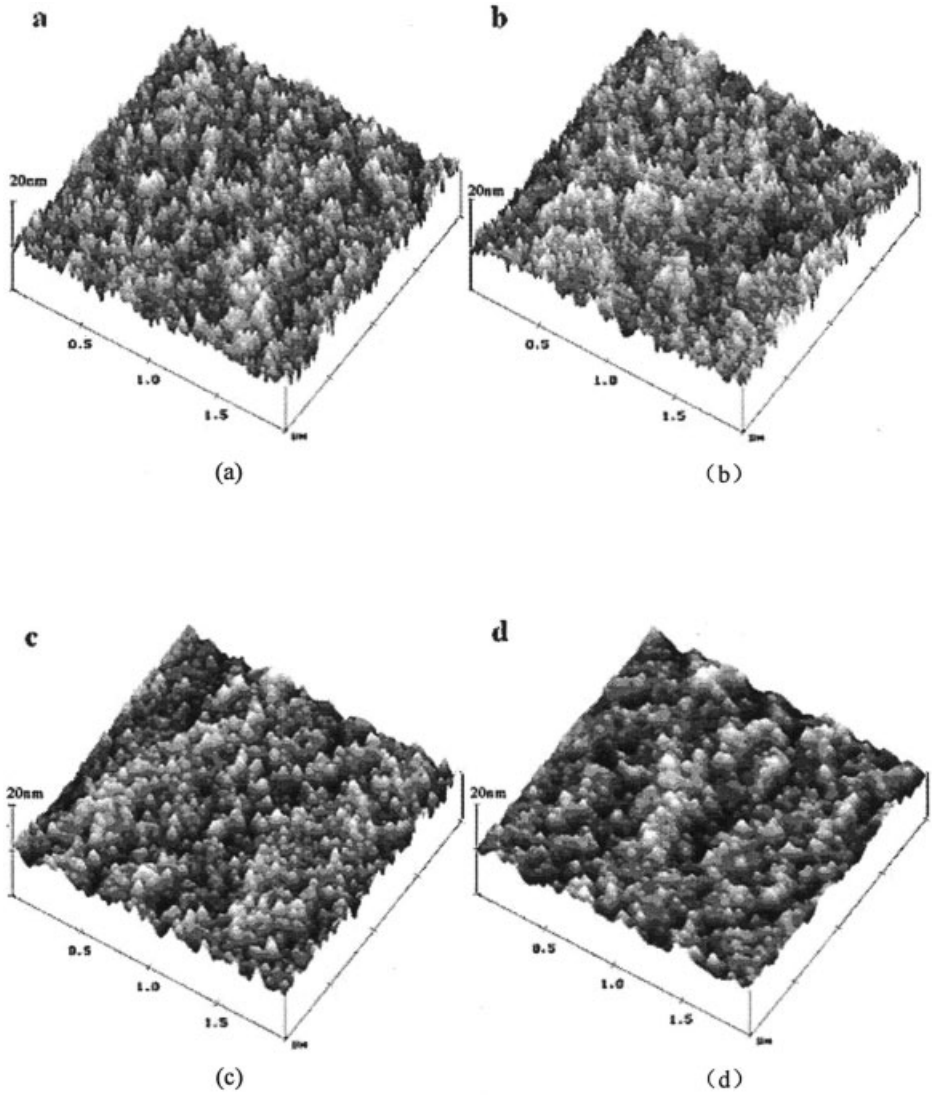

Figure 10 The AFM images of nanocomposite coats.

cles were modified first by MPS, then condensed and cured by UV under photoinitiator. The results showed that this process could form very smooth transparent films without any cracks. With increasing nanosilica particle size, the photopolymerization rate, final double bond conversion, and tack-free time of nanocomposites increased, while the surface roughness, glass-transition temperature, and UV absorbance of nanocomposites decreased. This process could be used to prepare organic–inorganic hybrid coats with high durability.

TABLE III
Surface Roughness of Nanocomposite Coats

	Coats with different nanosilica (nm)			
Rq (nm)	30	40	50	75
$2 \times 2\ \mu m^2$	2.4	2.3	1.7	1.4
$5 \times 5\ \mu m^2$	2.8	2.3	2.2	1.4

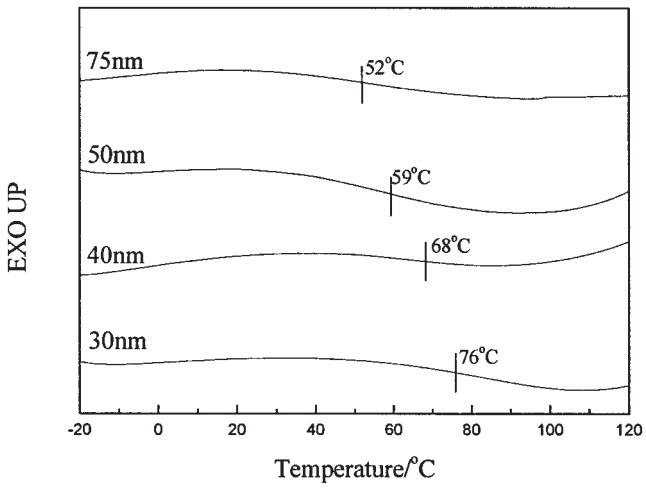

Figure 11 The DSC curves for nanocomposites.

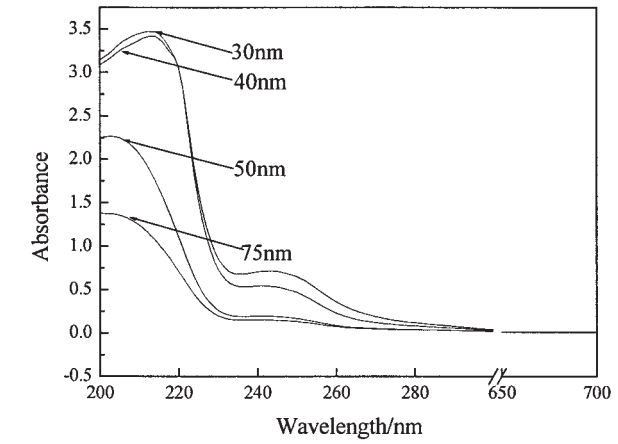

Figure 12 The UV–vis spectra of the nanocomposite coats: (a) absorbance; (b) transmittance.

References

1. Hwang, D. K.; Moon, J. H.; Shul, Y. G.; June, K. T.; Kim, D. H.; Lee, D. W. J Sol-Gel Sci Technol 2003, 26, 783.
2. Bauer, F.; Glasel, H. J.; Decker, U.; Ernst, H.; Freyer, A.; Hartmann, E.; Sauerland, V.; Mehnert, R. Prog Org Coat 2003, 47, 147.
3. Becker, O.; Varley, R. J.; Simon, G. P. Eur Polym J 2004, 40, 187.
4. Torre, L.; Frulloni, E.; Kenny, J. M.; Manferti, C.; Camino, G. J Appl Polym Sci 2003, 90, 2532.
5. Dong, W.; Zhu, C. Mater Lett 2000, 45, 336.
6. Bauer, F.; Ernst, H.; Decker, U.; Findeisen, M.; Glasel, H. J.; Langguth, H.; Hartmann, E.; Mehnert, R.; Peuker, C. Macromol Chem Phys 2000, 201, 2654.
7. Muh, E.; Stieger, M.; Klee, J. E.; Frey, H.; Mulhaupt, R. J Polym Sci Part A: Polym Chem 2001, 39, 4274.
8. Wenning, A. Macromol Symp 2002, 187, 597.
9. Soppera, O.; Croutxe-Barghorn, C. J Polym Sci Part A: Polym Chem 2003, 41, 716.
10. Decker, C. Polym Int 1998, 45, 133.
11. Vollath, D.; Szabo, D. V. Adv Eng Mater 2004, 3, 117.
12. Uhl, F. M.; Davuluri, S. P.; Wong, S. C.; Webster, D. C. Chem Mater 2004, 16, 1135.
13. Decker, C.; Zahouily, K.; Keller, L.; Benfarhi, S.; Bendaikha, T.; Baron, J. J Mater Sci 2002, 37, 4831.
14. Benfarhi, S.; Decker, C.; Keller, L.; Zahouily, K. Eur Polym J 2004, 40, 493.
15. Glasel, H. J.; Bauer, F.; Ernst, H.; Findeisen, M.; Hartmann, E.; Langguth, H.; Mehnert, R.; Schubert, R. Macromol Chem Phys 2000, 201, 2765.
16. Bauer, F.; Sauerland, V.; Glasel, H. J.; Ernst, H.; Findeisen, M.; Hartmann, E.; Langguth, H.; Marquardt, B.; Mehnert, R. Macromol Mater Eng 2002, 287, 546.
17. Bauer, F.; Sauerland, V.; Ernst, H.; Glasel, H. J.; Naumov, S.; Mehnert, R. Macromol Chem Phys 2003, 204, 375.
18. Andrzejewska, E. Prog Polym Sci 2001, 26, 605.
19. Xu, G.; Li, A.; Zhang, L.; Wu, G.; Yuan, X.; Xie, T. J Appl Polym Sci 2003, 90, 837.
20. Xiong, M.; You, B.; Zhou, S.; Wu, L. Polymer 2004, 45, 2967.
21. Wang, J. Z. Y.; Bogner, R. H. Int J Pharm 1995, 113, 113.
22. Li, F.; Zhou, S.; Gu, G.; You, B.; Wu, L. J Appl Polym Sci 2005, 96, 912.
23. Wei, H.; Lu, Y.; Shi, W.; Yuan, H.; Chen, Y. J Appl Polym Sci 2001, 80, 51.
24. Studer, K.; Decker, C.; Beck, E.; Schwalm, R. Prog Org Coat 2003, 48, 92.
25. Seubert, C. M.; Nichols, M. E.; Cooper, V. A.; Gerlock, J. L. Polym Degrad Stab 2003, 81, 103.